

Towards Adversarially Robust and Domain Generalizable Stereo Matching by Rethinking DNN Feature Backbones

Kelvin Cheng
North Carolina State University

Christopher Healey
North Carolina State University

Tianfu Wu
North Carolina State University

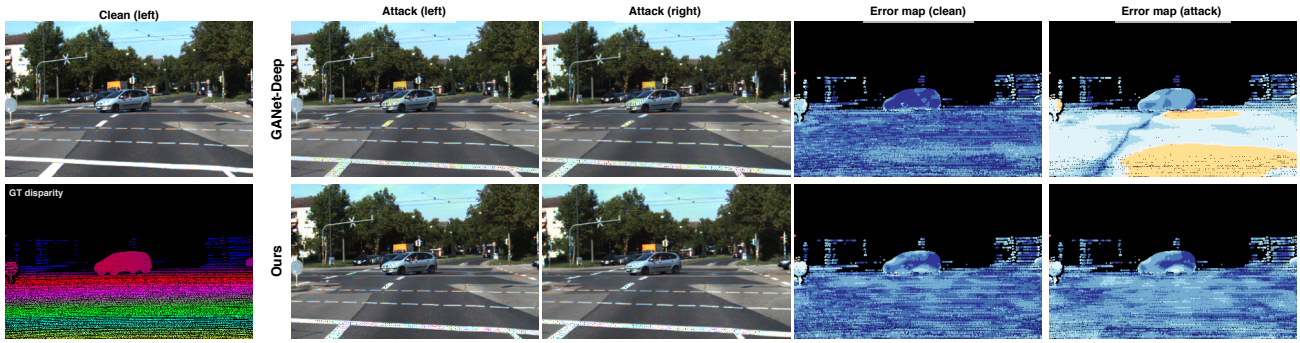


Figure 1. Examples of attacking stereo matching in the KITTI2015 [25] dataset. The attack is based on the proposed stereo-constrained projected gradient descent (PGD) attack (20 steps with $\epsilon = 0.06$), which is by design a type of weaker attacks to investigate the robustness of stereo matching methods. One of the state-of-the-art methods, GANet-Deep [44] shows a significant drop in performance (the last column), while the proposed method shows much stronger resistance to the attack. See text for detail.

Abstract

Stereo matching has recently witnessed remarkable progress using Deep Neural Networks (DNNs). But, how robust are they? Although it has been well-known that DNNs often suffer from adversarial vulnerability with a catastrophic drop in performance, the situation is even worse in stereo matching. This paper first shows that a type of weak white-box attacks can fail state-of-the-art methods. The attack is learned by a proposed stereo-constrained projected gradient descent (PGD) method in stereo matching. This observation raises serious concerns for the deployment of DNN-based stereo matching. Parallel to the adversarial vulnerability, DNN-based stereo matching is typically trained under the so-called simulation to reality pipeline, and thus domain generalizability is an important problem. This paper proposes to rethink the learnable DNN-based feature backbone towards adversarially-robust and domain generalizable stereo matching, either by completely removing it or by applying it only to the left reference image. It computes the matching cost volume using the classic multi-

scale census transform (i.e., local binary pattern) of the raw input stereo images, followed by a stacked Hourglass head sub-network solving the matching problem. In experiments, the proposed method is tested in the SceneFlow dataset and the KITTI2015 benchmark. It significantly improves the adversarial robustness, while retaining accuracy performance comparable to state-of-the-art methods. It also shows better generalizability from simulation (SceneFlow) to real (KITTI) datasets when no fine-tuning is used.

1. Introduction

1.1. Motivation and Objective

Inspired by the binocular vision system of human, stereo matching is a long-standing problem in computer vision that aims to recover 3D information from stereo image pairs, which has a great potential in a wide range of applications such as autonomous driving and robot autonomy. As its name suggests, this problem can be reduced to the problem of finding the correct corresponding pixel in the right image for each pixel in the left image. Although seemingly intu-

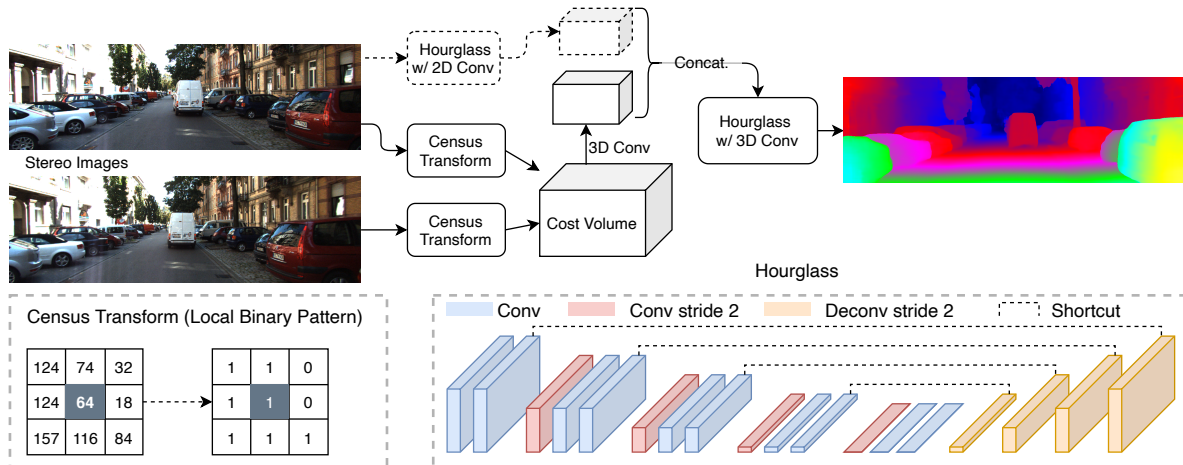


Figure 2. Illustration of the proposed minimally-simple workflow for stereo matching. The key difference between the proposed method and prior arts lies in the way of computing the cost volume. The proposed method harnesses the classic multi-scale census transform (left-bottom) of raw intensity of an input stereo image pair, while prior arts utilize features computed by a ConvNet feature backbone on an input stereo image pair. The proposed method also exploits ConvNet features computed only using the left reference image, as contextual information to the cost volume. Note that we also test the workflow without using the ConvNet feature context branch, that is to completely remove the ConvNet feature backbone. For the cost aggregation component, the proposed method utilizes a stacked Hourglass sub-network equipped with 3D convolution. Please see the text for detail.

itive, it has been studied for several decades due to the inherent difficulties of handling occlusions, repeated patterns, and textureless regions.

As in many other computer vision problems, Deep neural networks (DNNs) have made tremendous progress in stereo matching. Compared to traditional methods, DNNs not only enjoy a faster computation time, but also have a higher accuracy in public datasets [13, 25, 32]. Despite its success, it also faces challenges that can potentially harm its real world applications, such as autonomous driving. One of the biggest concerns is its adversarial vulnerabilities towards attacks [39, 21, 35, 12]. This situation has become critical as many powerful approaches have been developed where imperceptible perturbations to DNN inputs could deceive a well-trained DNN, significantly altering its prediction. Such results have initiated a rapidly proliferating field of research characterized by ever more complex attacks [15, 24, 28, 23, 41, 10, 45] that prove increasingly strong against defensive countermeasures [19, 40, 29]. *For the trade-off between accuracy and adversarial vulnerability, DNNs have become the Gordian Knot in state-of-the-art computer vision systems.*

Most of adversarial attack methods focus on a single image in image classification or object detection. As we shall show and as expected, one of the popular attack methods, the projected gradient descent (PGD) method [24], can easily deceive state-of-the-art stereo matching models when applied to the input image pair in the vanilla way [38]. However, such attack will violate the important underlying photometric consistency constraint of stereo matching, which refers to the property that the colors of corresponding

pairs should be similar except for occluded or specular regions, where either such matching does not exist (e.g. due to blocking), or the colors are naturally different because of the viewing angles. The term radiometric difference is used to describe the color difference of matching pairs [37]. Therefore, an attack that does not alter the radiometric difference can be considered as changing the textures of the objects in the scene, while the photometric consistency is maintained. For textureless regions such as a white wall, attacks can potentially add textures on the surfaces and "leak" the depth information. In general, extra textures are helpful for matching since they create more unique patterns, for example, researchers use human-invisible spectrum to create extra textures in infrared stereo systems. The important question is, with all these constraints and the fact that textures are helpful, can we still attack DNN-based stereo matching just by changing the textures of the objects in the scene? To this end, we propose the stereo-constrained PGD method, a considerably weaker attack, to test the adversarial vulnerability of DNN-based stereo matching methods and demonstrate that these attacks are still capable of deceiving DNNs (Fig. 1). This may suggest that DNN-based stereo matching methods are more vulnerable than we thought, and thus become more critical when applied in high-stakes applications such as autonomous driving.

To defend against adversarial attacks, most methods seek developing more complex DNNs (e.g., by adding denoising layers [40]) that are further adversarially trained [38]. Unlike the "growing" paradigm, we seek to "shrink" the design of DNN-based stereo matching methods, which often consists of three consecutive components: a feature back-

bone mapping raw images to a feature space, a cost volume defining the matching solution space using the learned features, and a head sub-network playing the role of a learnable optimizer that seeks the best matching result. On one hand, at a high-level, the learnability of adversarial attacks is contributed by the two aspects: the highly-expressive representational power of DNNs, and the fully differentiable pipeline. They enable the learning of attacks given a properly designed adversary loss function is used. So, we ask the question: *Can we shrink some differentiable components in the pipeline, that is to partially “cut off” the Gordian Knot?* This simple (and bold) strategy may cause a slight performance drop, but is entailed since recent work suggests there exists an inherent conflict between accuracy and robustness [34, 5]. On the other hand, as the name itself literally indicates, matching is the key challenge of stereo matching due to the large solution space. We hypothesize that the power of DNNs should devote to solve the optimization of the matching problem. Similar as traditional methods [17, 18], the solution space (i.e., the cost volume) can be directly defined based on raw input stereo images. To this end, we propose to rethink the DNN-based feature backbone towards adversarial robustness: either completely removing it or applying it only for the left reference image in a stereo pair to contextualize the cost volume (Fig. 2).

Parallel to the adversarial vulnerability, *cross-domain generalizability* also is an important problem in stereo matching: DNN-based stereo matching is typically pre-trained under the so-called simulation to real (Sim2Real) pipeline due to the high cost of collecting ground-truth matching results in practice and the data-hungry aspect of DNNs. It has been shown that DNNs may learn shortcut solutions that are strongly biased by the training dataset [14]. Removing or rewiring the DNN feature backbone in stereo matching may alleviate the opportunity of shortcut learning, and thus resulting in better performance in cross-domain deployment, especially when no fine-tuning is used. These are verified in our experiments from the SceneFlow dataset [27] to the KITTI benchmark [25] when no fine-tuning is used.

1.2. Method Overview

In this section, we give a brief overview of the proposed stereo matching model, which is a minimally-simple design that harnesses the best of the classic approaches and the state-of-the-art DNN-based approaches in stereo matching. Fig. 2 illustrates the proposed workflow.

Given an input pair of stereo images (rectified) and a pre-defined and fixed number of disparity levels, we first compute the cost volume based on the multi-scale census transform (i.e., local binary pattern features) of raw intensity of the stereo images. Census Transform was one of the best choices in traditional stereo matching [18, 2]. The cost volume is a 4-D tensor with the axes of height, width, disparity, and scale. Each entry of the cost volume represents the sim-

ilarity between a source pixel in the left reference image to the target pixel in the right image based on the disparity, and the similarity is computed using the Hamming distance between the census transform of the two local patches of the given scale size centered at the source and target pixels respectively. As an optional component, the cost volume is then concatenated with the ConvNet feature map computed only using the left reference image.

For cost aggregation in inferring the disparity map, unlike prior arts that often include hyper-parameters in the workflow to adapt to different scenes such as the smoothness among neighboring pixels, and/or sophisticated designs to connect ConvNet feature backbone and the cost aggregation sub-network, we adopt a fully-convolutional design using a 3-stack Hourglass sub-network equipped with 3D convolution for its capability of capturing long-range contextual information.

Adversarial robustness and cross-domain generalizability are facilitated by the proposed minimally-simple design of integrating the classic method of computing the cost volume and the state-of-the-art method of aggregating the cost, since the cost volume is based on multi-scale local rank information and Hamming distance.

Our Contributions. In summary, this paper makes three main contributions to the field of stereo matching: (i) It proposes a minimally-simple design for stereo matching, which shows significantly better adversarial robustness and cross-domain domain (Sim2Real) generalizability when no-fine tuning is used. (ii) It presents a stereo-constrained projected gradient descent (PGD) attack method, which by design learns weaker attacks to show the more serious vulnerability of state-of-the-art DNN-based stereo matching methods. (iii) It showcases a deep integrative learning paradigm by rethinking the end-to-end DNN feature backbones in stereo matching, which sheds light on potentially mitigating shortcut learning in DNNs via leveraging classic hand-crafted features if a problem-specific sweet spot can be identified (such as the cost volume in stereo matching).

2. Related Work

Stereo Matching. Before the recent resurgence of deep neural networks (DNNs), a traditional stereo matching algorithm usually involves four stages: matching cost computation, cost aggregation, optimization, and refinement [33, 18, 2]. While the recent DNN-based methods do not have these stages explicitly, efficient designs usually follow the same methodology [43, 27, 20, 6, 44]. We briefly review DNN-based stereo matching work.

In MC-CNN [43], Zbontar *et al.* developed the first deep learning approach for stereo matching and achieved great accuracy in many public datasets by using Siamese neural networks to compare the cost of two images’ patches in the stage of matching cost computation. However, their

approach is not end-to-end trainable. The comparison of all image patches will form a cost volume that can be further processed by Semi-Global Matching [17] to get the final disparity. In DispNet [27], Mayer *et al.* built the first end-to-end DNN-based method that can regress the disparity directly from two images. To overcome the lack of data, they constructed SceneFlow, a large-scale synthetic dataset with around 40,000 images. Nearly all subsequent DNN-based methods use the SceneFlow dataset for pre-training.

While previous approaches use a scalar cost at each disparity level, Kendall *et al.* proposed to expand the dimensions by concatenating features in the cost volume stage and to use 3D convolutional layers for cost aggregation in the GCNet [20]. They proposed a soft arg min operator that computes the expected disparity by treating the last layer of the cost aggregation stage as a disparity distribution. These design choices are very successful and most subsequent approaches [44, 16, 7] followed the same strategy.

Chang *et al.* [6], Du *et al.* [11], and Guo *et al.* [16] further improve deep learning approaches using different designs at the cost volume stage. Chang *et al.* proposed to use a Spatial Pyramid Pooling (SPP) Module for feature extraction and to use the stacked Hourglass structures [26] for the cost aggregation. With the proposed changes, their methods achieved better results while retaining end-to-end trainable. We also adopt the Hourglass structures in the design, but do not utilize the SPP module for simplicity.

Zhang *et al.* and Chen *et al.* proposed to propagate cost spatially in deep neural nets to reduce the number of 3D convolutional layers [44, 7]. They show that spatial propagation layers can be more parameter efficient than 3D convolutional layers at the same resolution. However, spatial propagation layers cannot replace all the 3D convolutional layers and still need to be used jointly to achieve great results. We only use 3D convolutions in aggregating costs for simplicity. In addition, Zhang *et al.* also use stacked Hourglass [26] for feature extraction. Cheng *et al.* applies Neural Architecture Search (NAS) techniques to automatically find optimal architectures for each stage and further improve the performance [8]. These approaches are the current state-of-the-art in the KITTI 2015 benchmark [25].

Besides accuracy, Yee *et al.* aimed at speeding up stereo matching by building the cost volume purely using highly optimized hand-crafted features (i.e. Census Transform and Sum of Absolute Differences) [42]. While our work also utilize Census Transform, they did not study adversarial attack and defense, and Sim2Real generalizability, which are our goals. The proposed work exploits deep integrative learning that combines multi-scale CT features and deep learning features, as well as the Hourglass networks in cost aggregation. In terms of accuracy, our KITTI2015 leader board result is better than Yee’s work (i.e. Bad 3.0: 2.39% vs 3.08%).

Adversarial Attacks. Assuming full access to DNNs pretrained with clean images, white-box targeted attacks are powerful ways of investigating the brittleness of DNNs. Many white-box attack methods focus on norm-ball constrained objective functions [36, 22, 4, 9, 31]. By introducing momentum in the MIFGSM method [9] and the ℓ_p gradient projection in the PGD method [24], they usually achieve better performance in generating adversarial examples.

In stereo matching, Wong *et al.* show the surprising fact that DNN-based stereo matching methods are vulnerable against unconstrained adversarial attacks [38]. However, without enforcing photometric consistency, vanilla attacks will violate the underlying physical properties of binocular vision and thus are not likely to happen in real life. For example, vanilla attacks cannot compute adversarial patches that can be produced in real life to fool stereo systems. Therefore we intentionally design the stereo-constrained PGD attack to further investigate the adversarial robustness with the presence of photometric consistency (Section 4). In terms of defense, they found that adversarial training can improve adversarial robustness against human-imperceptible FGSM attacks, but they did not experimented with the stronger PGD attacks nor adversarial patches. In contrast, we propose a new defense method that can significantly improve the adversarial robustness against adversarial patches and both unconstrained and stereo-constrained attacks without the need for adversarial training.

Another related work studied adversarial attacks in optical flow [30]. Optical flow tries to estimate object movements in consecutive frames in time. At a higher level, optical flow can be viewed as a more generalized matching problem in a sense that there are many corresponding pairs in consecutive frames. However, unlike in stereo matching, the positions of the pair are not limited to the same epipolar line. Also, colors of corresponding pairs can be drastically different due to different light source angles, viewing angles, or shading. Therefore, optical flow methods are inherently easier to attack. Besides the different natures of the two problems, their research did not propose new defense methods by utilizing the properties of optical flows. By leveraging the insights from Ranjan’s work, our work may shed light on studying more robust optical flow networks.

3. Approach

In this section, we first define the problem of stereo matching to be self-contained and with notations introduced. Then, we present the proposed minimally-simple method and a photometric-consistency constrained PGD attack method to evaluate the brittleness of DNN-based stereo matching methods.

3.1. Problem Formulation

Fig. 3 illustrates the stereo matching setup. The rectified left image is used as the reference image to infer the disparity map. For each pixel in the left image, the goal of stereo matching is to find the target pixel on the rectified epipolar line in the right image. The search range (i.e., disparity levels) often is predefined and fixed to a sufficiently large value in the cost volume computation stage. The matching is based on minimizing the cost between features centered at the source pixel and the target pixel respectively. The challenge of stereo matching is to seek the globally optimal matching for all pixels in the left reference image and to handle many uncertainties such as in the appearance features (textureless regions and specularities), the cost function, and unknown repeated patterns and occlusion situations.

Let Λ be an image lattice (e.g., 540×960) on which the rectified left and right images are defined, denoted by I^L and I^R respectively. Denote by $D(x, y)$ be the disparity map for the reference image I^L . In traditional methods, stereo matching is formulated as an energy/cost minimization problem,

$$\min_D E_d(I^L, I^R, D) + \lambda \cdot E_s(D), \quad (1)$$

where the first term is the data energy/cost, $E_d(I^L, I^R, D) = \sum_{(x,y) \in \Lambda} Cost(F_{I^L}(x, y), F_{I^R}(x + D(x, y), y))$ capturing the matching cost between a source pixel (x, y) in the left reference image and the target pixel $(x + D(x, y), y)$ on the rectified epipolar line (i.e., the same row) in the right image (the bottom of Fig. 3). The cost is measured based on features F_{I^L} and F_{I^R} extracted for the source and target pixel respectively. The second term represents the prior/regularity of a disparity map such as the pairwise smoothness assumption, $E_s(D) = \sum_{(u,v) \in \mathcal{N}} S(D(u), D(v))$ where $u, v \in \Lambda$ and \mathcal{N} the set of neighboring pixels (e.g., the 4-connected neighborhood). The challenges in the traditional formulation are in two-fold: what are the good features and the cost functions in the data term? And, what is the good prior that are sufficiently expressive to capture the disparity structures while facilitating efficient optimization (e.g., by the dynamic programming algorithm or semi-global method [17])?

Deep learning approaches mitigate the aforementioned challenges by exploiting the highly-expressive representational power and the end-to-end learning capability of DNNs. A cost volume is first computed which represents the solution space with respect to the data term in Eqn. 1. The prior/regularity term of a disparity map is made implicitly by the supervised loss function. The optimization algorithms (e.g., the traditional global or semi-global methods [17]) are also implicitly realized by a head sub-network (e.g., the stacked Hourglass sub-network in Fig. 2).

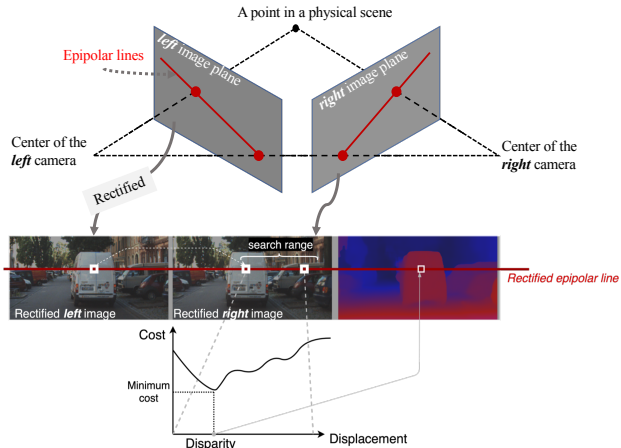


Figure 3. Illustration of stereo matching. *Top*: the stereo imaging setup consisting of two cameras capturing images of a physical scene. *Bottom*: Rectified images that are used in training and testing stereo matching models.

3.2. The Proposed Method

As illustrated in Fig. 2, the proposed workflow consists of three main components as follows.

Computing the Cost Volume Using Multi-Scale Census Transform. Most current stereo matching methods use DNN-based features to form the 4D cost volume. On one hand, DNN improves accuracy by providing a more unique feature for each pixel, but it also suffers from the inherent adversarial vulnerability. In contrast, traditional methods use similarity functions that are insensitive to local intensity changes [18, 2] and thus they are less likely to be affected by radiometric perturbations in nature. To eliminate the issue of radiometric differences caused by different exposure timing or non-Lambertian surfaces, previous studies find that Census Transform is the most robust and well-rounded cost function with global or semi-global methods [18, 2], which is inline with our need to be insensitive to local intensity changes that caused by adversarial perturbation in attacks. Therefore, we adopt Census Transform in computing the cost volume.

We use grey-scale raw intensity values in computing the census transform. Given a local window patch W centered at a pixel $u \in \Lambda$, the census transform computes the local binary pattern (the left-bottom in Fig. 2) by comparing each neighboring pixel $v \in W$ with u such that it equals 1 if $I(v) \geq I(u)$ and 0 otherwise. Hamming Distance (i.e. the number of different values in two bit strings) is used to compute the cost between two patches.

Unlike in traditional semi-global or global methods in which the cost of each pair can only a scalar, we take advantage of the flexibility of DNNs and design the multi-scale census transform to incorporate the context at different scales. Specifically, We use local windows with sizes from k_1 to k_2 (e.g. $k_1 = 3, k_2 = 11$ in our experiments) so

there are $K = k_2 - k_1 + 1$ (e.g., 9) costs associated with each matching candidate pairs. To normalize the cost at each scale, we divide the Hamming Distance by the number of pixels of each local window. For an input stereo image pair, I^L and I^R with the spatial dimensions $H \times W$, assume the maximum disparity level denoted by ℓ , the initial cost volume is a 4-D tensor of the size $H \times W \times \ell \times K$. To reduce the computational cost, we use 3D convolutions to down-scale the cost volume to be $1/3H \times 1/3W \times 1/3\ell \times C$, where $C = 32$ is the number of channels, as typically done by prior arts.

Contextualizing the Cost Volume and Aggregating the Cost. Although being robust to adversarial attacks, the census transform based cost volume alone is not sufficiently powerful to handle occlusion and more challenging semantic information, such as transparent objects and specular reflections. We introduce a 2-stack Hourglass module with 2D convolutions to extract context information from the left reference image, resulting in a $1/3H \times 1/3W \times C$ feature map which is unsqueezed along the second dimension (i.e., copying the feature map $1/3\ell$ times) to form a same size tensor as the down-scaled cost volume. The two are then concatenated along the second last dimension.

The contextualized cost volume will be fed into a 3-stack Hourglass module with 3D convolutions for the cost aggregation stage.

Disparity Map Prediction and the Loss Function. To predict the final disparity map $D(u), \forall u \in \Lambda$, the output of each stack in the Hourglass module of the cost aggregation is first up-sampled to the original size $H \times W \times \ell$, denoted as $D_s(x, y, d)$ where s is the stack index in the stacked Hourglass module. Then, similar to the method used in [20], the predicted disparity map $D_s(x, y)$ is computed by,

$$D_s(x, y) = \sum_{d=1}^{\ell} d \times \text{Softmax}(D_s(x, y, d)), \quad (2)$$

where Softmax is applied along the last dimension in $D_s(x, y, d)$.

In training, we use the smooth L_1 loss due to its robustness at disparity discontinuities and low sensitivity to outliers [6, 44]. Given the ground-truth disparity map $D^*(u)$, the loss is defined by,

$$\text{Loss}(\Theta; D^*) = \sum_{s=1}^S \beta_s \cdot \frac{1}{|\Lambda|} \sum_{u \in \Lambda} \text{Smooth}_{L_1}(D_s(u) - D^*(u)), \quad (3)$$

where Θ collects all parameters in our model, β_s represents the weight for the output from a stack s (e.g., 0.5, 0.7, and 1 are used for the 3-stack Hourglass module in our experiments), $u = (x, y) \in \Lambda$, and the smooth L_1 function is defined by,

$$\text{Smooth}_{L_1}(z) = \begin{cases} \frac{z^2}{2}, & \text{if } z < 1 \\ |z| - 0.5, & \text{otherwise.} \end{cases} \quad (4)$$

4. Stereo Constrained PGD Attacks

To study the brittleness of DNN based stereo matching models, we intentionally develop a weaker attacking method based on the PGD method [24], which retains the underlying photometric-consistency in stereo matching by changing the intensities of the same physical point in both images. More specifically, in learning attacks, the same amounts of perturbations are added to each pair of correspondence pixels in the left and right images simultaneously while occluded areas will not be modified. Since the left image is the reference image for computing the disparity loss, we disallow to attack and evaluate occluded regions of the reference image, which prevents the perturbation to attack the regions where the estimation does not rely on matching. Nonetheless, it is still possible to make perturbation on the occluded regions of the right image to hinder the matching, e.g. by creating false positive correspondence. Therefore we will show two versions of the attack in the experiment section, where one disallows to attack the occluded regions of the left image, and the other one disallows the occluded regions of both the left and right images to be attacked.

Given a perturbation map $P(x, y), \forall (x, y) \in \Lambda$, the distorted intensities for each pixel location (x, y) are computed as:

$$I_{adv}^L(x, y) = I^L(x, y) + P(x + D(x, y), y) \quad (5)$$

$$I_{adv}^R(x, y) = I^R(x, y) + P(x, y),$$

where $D(x, y)$ is either the ground-truth disparity map or the predicted one using the clean images. This is a weaker attack since we actually leak the underlying disparity information to the algorithm using the pair $(P(x, y), P(x + D(x, y), y))$ which may potentially help the stereo matching.

We use the L_∞ norm to measure similarities between images. Two images will appear visually identical under a certain threshold. To learn a L_∞ bounded adversarial perturbation P^{adv} , the iterative PGD method is used,

$$P_{t+1}^{adv} = \text{clip}_P^\epsilon \{ P_t^{adv} + \alpha \cdot \text{sign}(\nabla_P L(P_t^{adv})) \}, \quad (6)$$

where $t = 1, 2, \dots, T$ and P_0^{adv} starts with all zeros. L denotes the mean absolute error between the predicted disparity map for the perturbed images and the ground-truth disparity map or the disparity map predicted for the clean images. And, clip_P^ϵ clips the perturbation to be within the ϵ -ball of the corresponding zero-plane. Through out our experiments, we set $\epsilon = 0.06$ or 0.03 , $\alpha = 0.01$, and $T = 20$.

Attack Census Transform: Since Census Transform contains the non-differentiable comparison operator, the gradients from the constructed cost volume cannot be back-propagated directly to the input images and thus leading to an obfuscated gradient problem [1]. For non-differentiable operators, we can find differentiable alternatives to keep the gradient flows. Therefore, we combine subtraction and the sigmoid function as a differentiable approximation of the

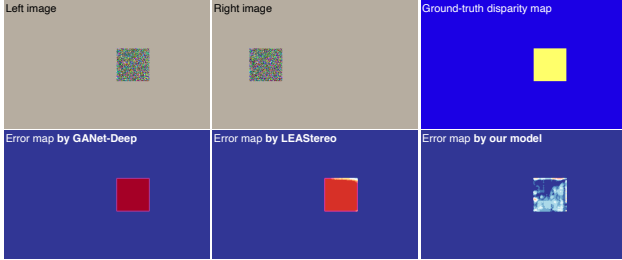


Figure 4. Illustration of adversarial vulnerability of deep stereo matching methods using a toy example: GANet-Deep [44], LEAStereo [8], and the proposed method. See text for detail.

comparison operator. As suggested in [1], we should perform the usual forward pass through the comparison operator, but compute the gradients through the differentiable combination of subtraction and the sigmoid function on the backward pass. However, as the derivative of the sigmoid function is $(1 - x)x$, a boolean value (0 or 1) will make it zero, and thus blocking the gradient flow. Therefore, we use the sigmoid in the forward pass as well and multiply the inputs by a large constant (e.g. 10^5) such that the output of the sigmoid function is close to either zero or one, while maintaining the gradient flow.

Robustness of Census Transform From the perspective of attacks, the binary patterns generated by Census Transform is harder to alter due to the comparison operator. Given a threshold of maximum pixel difference in perturbation, some neighbors will not be altered if their difference with the center is larger than twice of the threshold. If the attack does not violate photometric-consistency, it will be even harder to alter the cost between binary patches of corresponding pairs. Specifically, if a neighboring pixel appear in both the left and the right binary patches, its relative magnitude relationship with the center pixel will be the same for both patches, no matter how its intensities change. It is our interest to test if this highly non-linear operators can defend the DNNs against attacks.

5. Experiments

Data. We evaluate our method on the SceneFlow [27] and KITTI2015 [25] datasets. The SceneFlow dataset is a large-scale synthetic dataset that contains 35,454 training images and 4,370 test images at the resolution of 540×960 . Since it provides dense ground-truth disparities, it is widely used for pretraining DNN-based stereo matching methods. the KITTI2015 dataset is a real-world dataset of driving scenes, which contains 200 training images and 200 test images at the resolution of 375×1242 . Since the depth of each scene is obtained through LiDAR, the ground truth is not dense. In addition, we also test pretrained models on the Middlebury [32] dataset at quarter resolution.

Implementation Details. Our method is implemented in PyTorch and trained end-to-end using the Adam optimizer

Models	Clean / After Attack, (EPE [px])				
	$\ell=20$	60	100	140	180
PSMNet [6]	1.89/78.85	1.22/63.57	0.45/3.29	0.94/4.59	0.48/36.10
GANet-Deep [44]	2.36/9.94	6.74/27.72	7.37/80.39	13.56/115.77	15.09/31.95
LEAStereo [8]	0.54/31.86	0.32/1.13	0.36/1.18	0.33/98.23	0.96/146.68
Ours	0.36/3.12	0.28/5.56	0.13/0.44	0.37/9.47	0.094/1.77
Ours w/o backbone	0.057/0.051	0.20/0.20	0.29/0.25	0.25/0.24	0.26/0.26

Table 1. Result comparisons on synthetic adversarial patches at different disparity levels ℓ .

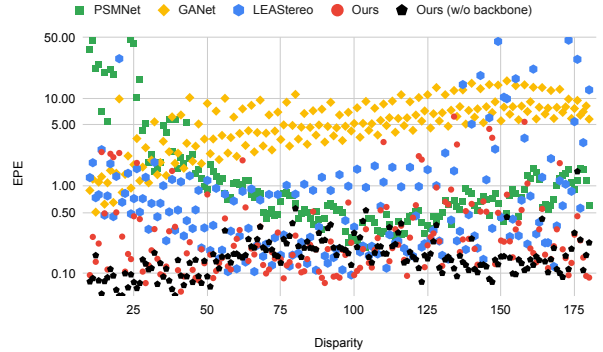


Figure 5. Test results of shifting an adversarial patch on the left image at disparities from 10 to 180, while fixing the right image. Each point represents a testing pair with a different displacement.

with $\beta_1 = 0.9$ and $\beta_2 = 0.999$. All images are preprocessed with color normalization. During training, we use a batch size of 8 on four GPUs using 240×576 random crops from the input images. The maximum disparity level is set to 192 and any values larger than this threshold will be ignored during training. *For SceneFlow*, we train our model from random initialization for 20 epochs with a constant learning rate of 0.001. *For KITTI2015*, we split the 200 training images into a training set of 140 images and a validation set of 60 images. We finetune our model pretrained on SceneFlow for another 600 epochs and use the validation set to select the best model. If no feature backbone is used to extract context information from the left image (Fig. 2), our model is denoted as “ours w/o backbone” in tables and figures.

Evaluation Metrics. We adopt the provided protocols in the two datasets. There are three metrics: **EPE [px]** which measures the end-point error in pixels, **Bad 1.0 [%]** and **Bad 3.0 [%]** which represents the error rate of errors larger than 1 pixel and 3 pixels respectively.

Baseline Methods. We compare with state-of-the-art deep stereo matching methods: the PSMNet [6], the GANet [44], and the LEAStereo [8]. We use their publicly released codes and trained model checkpoints in comparisons.

5.1. A Toy Experiment

Before showing the experimental results in SceneFlow and KITTI, we conduct a toy experiment that shows state-of-the-art stereo matching methods can be easily attacked even by a weaker attacking method (Fig. 4).

We create five synthetic toy stereo image pairs. In a

Models	Clean (Non-occlusion regions)			After PGD Attack ($\epsilon = 0.03$)			After PGD Attack ($\epsilon = 0.06$)		
	EPE	Bad 1.0	Bad 3.0	EPE	Bad 1.0	Bad 3.0	EPE	Bad 1.0	Bad 3.0
PSMNet [6]	1.56	20.62	5.36	12.37	68.12	30.75	25.51	75.66	51.13
GANet-Deep [44]	1.04	10.82	3.37	11.52	51.47	36.10	28.54	72.75	64.03
LEAStereo [8]	1.03	8.87	2.69	12.12	55.69	33.82	22.30	68.04	53.63
Ours	1.02	8.85	3.28	9.87	31.94	25.67	20.74	45.84	41.37
Ours w/o backbone	1.16	9.49	3.55	9.23	30.61	25.15	10.85	32.88	27.84
Ours [†]	1.02	8.85	3.28	2.25	12.64	6.71	5.79	18.09	13.04

Table 2. Stereo-Constrained 20-step PGD Attack Results in SceneFlow [27]. [†] shows results by our method without using the modified census transform in learning attacks (Sec. 4), which are much more resistant to attacks. See text for detail.

Models	Clean (Non-occlusion regions)			After PGD Attack ($\epsilon = 0.03$)			After PGD Attack ($\epsilon = 0.06$)		
	EPE	Bad 1.0	Bad 3.0	EPE	Bad 1.0	Bad 3.0	EPE	Bad 1.0	Bad 3.0
PSMNet [6]	1.56	20.62	5.36	12.32	68.15	30.76	20.15	74.50	46.74
GANet-Deep [44]	1.04	10.82	3.37	14.37	57.90	42.03	23.59	69.28	57.90
LEAStereo [8]	1.03	8.87	2.69	9.32	54.86	31.16	16.51	64.26	45.77
Ours	1.02	8.85	3.28	11.70	35.36	29.56	16.08	42.14	37.21
Ours w/o backbone	1.16	9.49	3.55	11.63	34.18	29.26	13.09	36.55	32.21

Table 3. Stereo-Constrained 20-step PGD Attack Results in SceneFlow [27]. Attacks on occluded regions of both the left and the right image are disallowed.

stereo pair, the left reference image is composed by superposing a white-noise patch onto a constant background. The right image is created using the same patch and the same background in which the patch is horizontally shifted with respect to a given disparity level (such as $\ell = 20$). So, the ground-truth disparity for the entire patch will be the specified ℓ . The background is excluded from the evaluation.

As shown in Table 1, for the clean synthetic images, state-of-the-art stereo matching methods work very well using the SceneFlow trained model checkpoints. Our model shows better performance for all disparity levels. After applying the proposed stereo-constrained PGD attack only to the patches (similar in spirit to the adversarial patches [3]), state-of-the-art methods’ performance drop significantly except for the LEAStereo method [8] at two disparity levels (60 and 100). Fig. 5 further shows the effects of applying the same adversarial patch at different disparity levels.

Through this toy experiment, we can observe: (i) Although not trained with this synthetic setting, state-of-the-art stereo matching methods are capable of recovering matching results when no attacks are applied. (ii) However, the matching capabilities are not stable even with respect to the much weaker stereo-constrained attacks. This may indicate that state-of-the-art methods could learn shortcut solutions in computing the cost volume, while our methods that directly utilize local rank information in computing the cost volume are more robust, either with or without the feature backbone in computing the cost volume.

5.2. Results in SceneFlow

We first compare the adversarial robustness. Table 2 and Table 3 shows the comparisons: **our models are much more robustness than prior arts**. As the original SceneFlow dataset does not have ground truth occlusion, we use

Models	Params [M]	EPE [px]	Bad 1.0 [%]	Bad 3.0 [%]
PSMNet [6]	3.5M	1.49	20.6	5.9
GANet-Deep [44]	6.6M	0.82	9.0	3.5
LEAStereo [8]	1.8M	0.83	8.0	3.3
Ours	2.7M	0.84	8.8	3.7
Ours w/o backbone	1.9M	1.10	9.7	4.4

Table 4. Result comparisons using clean images in the SceneFlow dataset [27].

a subset provided by the same authors [27] with occlusions. We randomly select 1,000 images from the test data. Our methods show significantly better robustness against attacks. In fact, our methods are the best in all metrics except for EPE in ScenFlow with $\epsilon = 0.03$ in Table 3. We note that if we do not allow to modify the model itself in learning white-box attacks, our method shows much better robustness, thanks to the non-differentiable cost volume computation. For obtaining a deeper understanding of the robustness problem, we will compare the “worst case” scenarios of the proposed method with the plain scenarios of prior arts in accessing adversarial robustness throughout the subsequent experiments

We also compare the results using the entire image, instead of only non-occlusion regions in evaluating attack performance. Table 4 shows the comparisons. Our method obtains competitive performance against state-of-the-art methods. Recent work suggests there exists an inherent conflict between accuracy and robustness [34, 5]. From this perspective, the comparable performance on clean images and the significantly better robustness of our method show that the proposed minimally-simple workflow for stereo matching is effective.

5.3. Sim2Real Cross-Domain Generalizability

To verify the conjecture that cross-domain generalizability in stereo matching can be induced by removing

Models	EPE [px]	Bad 1.0 [%]	Bad 3.0 [%]
PSMNet [6]	6.89	72.93	31.55
GANet-Deep [44]	1.66	42.12	10.48
LEAStereo [8]	2.00	51.29	13.90
Ours	1.26	27.92	6.31
Ours w/o backbone	1.25	25.95	6.12

Table 5. Results in the KITTI2015 [25] training dataset directly using SceneFlow pretrained models *without* fine-tuning.

Models	EPE [px]	Bad 1.0 [%]	Bad 3.0 [%]
PSMNet [6]	5.90	71.59	28.42
GANet-Deep [44]	1.48	31.61	9.51
LEAStereo [8]	1.91	44.26	14.28
Ours	1.28	20.62	7.16
Ours w/o backbone	1.23	19.66	6.80

Table 6. Results in the KITTI2012 [25] training dataset directly using SceneFlow pretrained models *without* fine-tuning.

Models	EPE [px]	Bad 1.0 [%]	Bad 3.0 [%]
PSMNet [6]	4.33	73.01	19.01
GANet-Deep [44]	2.26	27.45	11.40
LEAStereo [8]	3.47	32.67	14.81
Ours	1.96	20.09	10.05
Ours w/o backbone	1.71	18.72	9.16

Table 7. Results in the Middlebury [32] training dataset at quarter resolution directly using SceneFlow pretrained models *without* fine-tuning.

the dependency between the cost volume computation and the learnable feature backbone, we evaluate all models pretrained on SceneFlow directly on the KITTI training datasets and the Middlebury training dataset [32]. As shown in Table 5, 6, and 7, **our method outperforms prior arts by a large margin**. This result shows that exploiting a non-parametric cost volume not only improves adversarial robustness, but also enhances the Sim2Real cross-domain generalizability.

Besides our method, it is interesting to see that the GANet [44] has a stronger generalization ability than others. This result suggests that the semi-global aggregation layer in GANets can generalize better than solely using convolutional layers. *Since our method does not utilize any special layers in the cost aggregation, the generalization ability can only come from the more cross-domain consistent cost volume formed by the multi-scale census transform.*

5.4. Results in KITTI

Since the entire training set in KITTI2015 consists of 200 images, different methods use different training strategies. Based on the information available, GANets [44], PSMNets [6], and our method use 200, 160, 140 images respectively in fine-tuning. The setting of the LEAStereo method [8] is not publicly available. The train-val splits used in fine-tuning by different methods also are not publicly available and thus may be inconsistent. We empirically observe that different methods including ours show overfitting tendency in fine-tuning due to the limited data.

Adversarial Robustness Comparisons. To evaluate the adversarial robustness in KITTI2015, we directly test the

trained models on the entire training dataset (200 images). Since the ground truth disparities in KITTI2015 are not dense, only those non-occluded pixels with ground truths are used in learning attacks. Therefore, the number of pixels that can be attacked in KITTI2015 is significantly less compared to SceneFlow. Due to the GPU memory limitation, we only use the 240×384 center part of each image. Because of cropping, we also ignore those pixels where their correspondences are outside of the cropped images. Table 8 and Table 9 show the comparison results. **Our method shows significantly better robustness. The overall improvement is more significant than the improvement in SceneFlow** (Table 2).

To show the proposed stereo-constrained PGD attack is indeed a type of weaker attack, we also conduct experiments using the vanilla PGD attacking method that learns the perturbation to both the left image and the right image in the vanilla way. Table 10 shows the results verifying the claim, compared to those in Table 8.

Adversarial Patch Attack To test if the adversarial vulnerability can be intentionally exploited in a more realistic setting, such as autonomous driving, We extend the patch attack experiment (Section 5.1) to demonstrate the possibility of such attempts.

We select two scenarios where the adversarial patches can be put on more flat surfaces. To simulate the effects of "sticking" the adversarial patches on the surface, the ground truth disparities of the patches are the same as the corresponding part of the original image. For each image pair, we apply stereo-constrained PGD attacks with 1,000 iterations, the results are shown in Figure 6. The first row shows the attacked image pairs. Our method, LEAStereo [8], and GANet-Deep [44] are shown on the second, third, and fourth row respectively. The first and the third columns are the after attack disparity maps, and the second and the fourth columns are the after attack error maps from the predictions.

We can see that the disparity maps are largely altered for LEAStereo and GANet, making the affected surfaces much closer than they really are. For LEAStereo, the EPEs of the whole images are dropped from 0.35 to 1.13 and from 0.48 to 6.79. EPEs of GANet are dropped from 0.20 to 2.69 and from 0.28 to 7.96. For our method, the EPEs are only dropped slightly from 0.32 to 0.39 and from 0.42 to 0.57.

Ablation Study The census transform (CT) is chosen due to its non-differentiability and the fact that it is a well-rounded choice in the literature. We use multi-scale representations to respect the common recognition of its expressivity, and to alleviate choosing window size as a dataset-dependent hyper-parameter. We compare with traditional Sum of Absolute Difference (SAD) and show the results in Table 12. We can see that CT is indeed much more robust than SAD due to its non-differentiability. CT with multi-

Models	Clean			PGD Attack ($\epsilon = 0.03$)			PGD Attack ($\epsilon = 0.06$)		
	EPE	Bad 1.0	Bad 3.0	EPE	Bad 1.0	Bad 3.0	EPE	Bad 1.0	Bad 3.0
PSMNet [6]	0.28	2.00	0.16	29.05	84.75	54.85	84.04	90.41	83.68
GANet-Deep [44]	0.25	1.42	0.10	3.93	70.64	29.94	9.75	84.68	68.70
LEAStereo [8]	0.37	4.54	0.42	4.02	71.20	29.09	11.38	83.24	63.61
Ours	0.36	3.61	0.27	0.89	22.18	3.76	3.68	53.44	19.57
Ours w/o backbone	0.38	4.14	0.32	1.13	24.64	2.46	1.43	30.69	8.05

Table 8. Stereo-Constrained 20-step PGD Attack Results in the KITTI2015 training dataset [25]. Note that on clean images, the results by GANet-Deep are training performance; the results by PSMNet and our method include 40 and 60 validation images respectively.

Models	Clean			PGD Attack ($\epsilon = 0.03$)			PGD Attack ($\epsilon = 0.06$)		
	EPE	Bad 1.0	Bad 3.0	EPE	Bad 1.0	Bad 3.0	EPE	Bad 1.0	Bad 3.0
PSMNet [6]	0.28	2.00	0.16	1.29	45.79	5.12	5.19	70.73	30.08
GANet-Deep [44]	0.25	1.42	0.10	1.25	39.76	5.92	2.93	63.88	25.84
LEAStereo [8]	0.37	4.54	0.42	1.44	46.57	7.61	3.20	66.26	27.45
Ours	0.36	3.61	0.27	0.53	9.90	0.75	0.59	11.97	0.93
Ours w/o backbone	0.38	4.14	0.32	0.60	12.95	1.16	0.64	14.39	1.42

Table 9. Stereo-Constrained 20-step PGD Attack Results in the KITTI2015 training dataset [25]. Attacks on occluded regions of both the left and the right image are disallowed.

Models	PGD Attack ($\epsilon = 0.03$) w/ GT			PGD Attack ($\epsilon = 0.03$) w/ Prediction		
	EPE [px]	Bad 1.0 [%]	Bad 3.0 [%]	EPE [px]	Bad 1.0 [%]	Bad 3.0 [%]
PSMNet [6]	91.08	92.75	89.91	58.75	84.11	70.49
GANet-Deep [44]	23.75	89.48	79.11	19.49	68.01	51.58
LEAStereo [8]	14.71	82.42	64.31	12.03	74.21	54.00
Ours	1.81	36.42	11.29	1.53	29.25	10.09
Ours w/o backbone	2.36	41.34	16.30	2.27	34.98	14.74

Table 10. Vanilla 20-step PGD Attack Results in the KITTI2015 training dataset [25]. The PGD attacks are learned using either the GT disparity map or the predicted disparity map from clean images in the loss function used to compute PGD. The performance are still measured in terms of the GT disparity map.

Models	Bad 3.0 [%]		Non-Occlusion		All Areas	
	FG	Avg All	FG	Avg All	FG	Avg All
GCNet [20]	5.58	2.61	6.16	2.87		
PSMNet [6]	4.31	2.14	4.62	2.32		
GANet-15 [44]	3.39	1.84	3.91	2.03		
GANet-Deep [44]	1.34	1.63	1.48	1.81		
LEAStereo [8]	2.65	1.51	2.91	1.65		
Ours	3.54	2.09	4.16	2.39		

Table 11. KITTI2015 leaderboard comparison results. FG means foreground regions.

ple scales has a stronger robustness than the single-scale version, while having a slightly better accuracy due to its flexibility, which is as expected.

Models	SceneFlow		KITTI15 (pretrained)		KITTI15 Attack ($\epsilon = 0.03$)	
	EPE [px]	Bad 3.0 [%]	EPE [px]	Bad 3.0	EPE [px]	Bad 3.0 [%]
multi-scale SAD	1.02	4.02	1.71	9.69	2.30	18.20
CT (w=11)	1.18	4.77	1.28	6.38	1.88	7.22
Ours	0.84	3.70	1.26	6.31	0.89	3.76
Ours w/o backbone	1.10	4.40	1.25	6.12	1.13	2.46

Table 12. Comparison with CT with window size 11 and multi-scale SAD

Leaderboard Comparisons. Table 11 shows the comparisons. Our method is slightly worse than state-of-the-art methods. As aforementioned, the detail of fine-tuning the SceneFlow pretrained model may play a significant role in the leaderboard comparisons. Our method is only fine-tuned by 140 training images in a vanilla manner with any bells and whistles. The gap may be bridged if more ablation

studies are conducted. We will also seek more computing resources to conduct more consistent and fair comparisons by re-training the prior arts using their officially released codes with the same settings.

6. Conclusions

This paper presents a minimally-simple workflow for stereo matching, which harnesses the best of classic features (multi-scale census transform) and end-to-end trainable DNNs for adversarially-robust and cross-domain generalizable stereo matching. The proposed method is motivated by the observation that DNN-based stereo matching methods can be deceived by a type of weaker attacks that entail stereo constraints in learning the perturbation. To address the adversarial vulnerability, this paper proposes to rethink the DNN feature backbone used in computing the cost volume: either completely removing it or rewiring it to extract contextual information from only the reference (left) image. In experiments, the proposed method is tested in SceneFlow and KITTI2015 datasets with significantly better adversarial robustness and Sim2Real cross-domain generalizability (when no fine-tuning is used) achieved. It also obtains on-par performance on clean images.

Acknowledgements

This work is supported in part by NSF IIS-1909644, ARO Grant W911NF1810295, NSF IIS-1822477, NSF CMMI-2024688, NSF IUSE-2013451, DHHS-ACL Grant 90IFDV0017-01-00 and the GIFT fund from the InnoPeak Technology, Inc.. The views presented in this paper are those of the authors and should not be interpreted as representing any funding agencies.

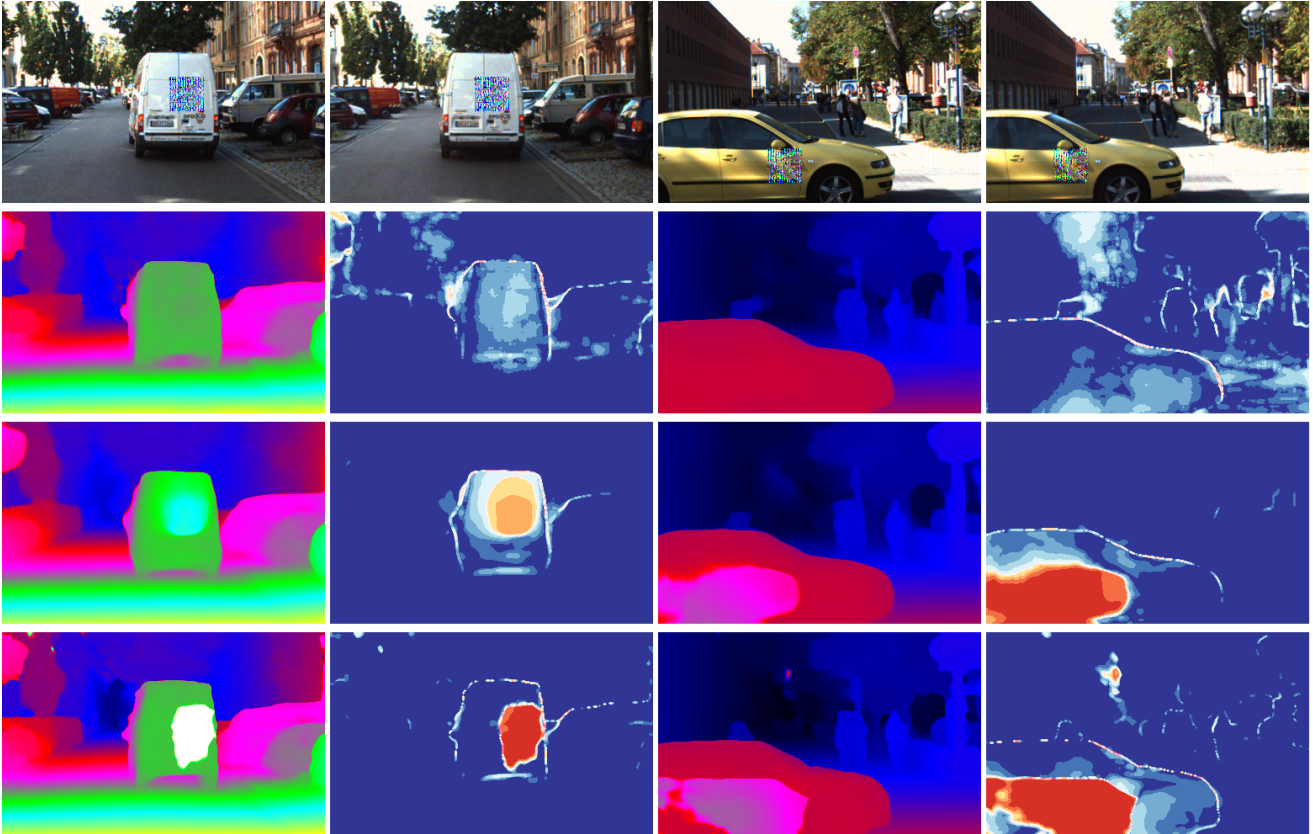


Figure 6. Illustration of the adversarial patch attack.

References

- [1] Anish Athalye, Nicholas Carlini, and David Wagner. Obfuscated gradients give a false sense of security: Circumventing defenses to adversarial examples. In Jennifer Dy and Andreas Krause, editors, *Proceedings of the 35th International Conference on Machine Learning*, volume 80 of *Proceedings of Machine Learning Research*, pages 274–283, Stockholm, Sweden, 10–15 Jul 2018. PMLR.
- [2] Michael Bleyer and Sylvie Chambon. Does color really help in dense stereo matching. Citeseer, 2010.
- [3] Tom B Brown, Dandelion Mané, Aurko Roy, Martín Abadi, and Justin Gilmer. Adversarial patch. *arXiv preprint arXiv:1712.09665*, 2017.
- [4] Nicholas Carlini and David A. Wagner. Towards evaluating the robustness of neural networks. In *2017 IEEE Symposium on Security and Privacy, SP 2017, San Jose, CA, USA, May 22-26, 2017*, pages 39–57, 2017.
- [5] Yair Carmon, Aditi Raghunathan, Ludwig Schmidt, and John Duchi. Unlabeled data improves adversarial robustness. *Advances in neural information processing systems*, 2019.
- [6] Jia-Ren Chang and Yong-Sheng Chen. Pyramid stereo matching network. In *Proc. of IEEE Conference on Computer Vision and Pattern Recognition (CVPR)*, pages 5410–5418, 2018.
- [7] Xinjing Chen, Peng Wang, and Ruigang Yang. Learning depth with convolutional spatial propagation network. *arXiv*, 2018.
- [8] Xuelian Cheng, Yiran Zhong, Mehrtash Harandi, Yuchao Dai, Xiaojun Chang, Hongdong Li, Tom Drummond, and Zongyuan Ge. Hierarchical neural architecture search for deep stereo matching. *Advances in Neural Information Processing Systems*, 33, 2020.
- [9] Yinpeng Dong, Fangzhou Liao, Tianyu Pang, Hang Su, Jun Zhu, Xiaolin Hu, and Jianguo Li. Boosting adversarial attacks with momentum. In *CVPR*, pages 9185–9193. IEEE Computer Society, 2018.
- [10] Yinpeng Dong, Tianyu Pang, Hang Su, and Jun Zhu. Evading defenses to transferable adversarial examples by translation-invariant attacks. In *IEEE Conference on Computer Vision and Pattern Recognition, CVPR 2019, Long Beach, CA, USA, June 16-20, 2019*, pages 4312–4321, 2019.
- [11] Xianzhi Du, Mostafa El-Khamy, and Jungwon Lee. Amnet: Deep atrous multiscale stereo disparity estimation networks. *arXiv*, 2019.
- [12] Javid Ebrahimi, Anyi Rao, Daniel Lowd, and Dejing Dou. Hotflip: White-box adversarial examples for text classification. In *Proceedings of the 56th Annual Meeting of the Association for Computational Linguistics, ACL 2018, Mel-*

- bourne, Australia, July 15-20, 2018, Volume 2: Short Papers, pages 31–36, 2018.
- [13] Andreas Geiger, Philip Lenz, and Raquel Urtasun. Are we ready for autonomous driving? the kitti vision benchmark suite. In *Proc. of IEEE Conference on Computer Vision and Pattern Recognition (CVPR)*, 2012.
- [14] Robert Geirhos, Jörn-Henrik Jacobsen, Claudio Michaelis, Richard Zemel, Wieland Brendel, Matthias Bethge, and Felix A Wichmann. Shortcut learning in deep neural networks. *Nature Machine Intelligence*, 2(11):665–673, 2020.
- [15] Ian J. Goodfellow, Jonathon Shlens, and Christian Szegedy. Explaining and harnessing adversarial examples. In *3rd International Conference on Learning Representations, ICLR 2015, San Diego, CA, USA, May 7-9, 2015, Conference Track Proceedings*, 2015.
- [16] Xiaoyang Guo, Kai Yang, Wukui Yang, Xiaogang Wang, and Hongsheng Li. Group-wise correlation stereo network. In *Proc. of IEEE Conference on Computer Vision and Pattern Recognition (CVPR)*, 2019.
- [17] H. Hirschmuller. Accurate and efficient stereo processing by semi-global matching and mutual information. In *2005 IEEE Computer Society Conference on Computer Vision and Pattern Recognition (CVPR'05)*, volume 2, pages 807–814 vol. 2, 2005.
- [18] Heiko Hirschmuller and Daniel Scharstein. Evaluation of stereo matching costs on images with radiometric differences. *IEEE Transactions on Pattern Analysis and Machine Intelligence*, 31(9):1582–1599, 2008.
- [19] Harini Kannan, Alexey Kurakin, and Ian J. Goodfellow. Adversarial logit pairing. *CoRR*, abs/1803.06373, 2018.
- [20] Alex Kendall, Hayk Martirosyan, Saumitro Dasgupta, Peter Henry, Ryan Kennedy, Abraham Bachrach, and Adam Bry. End-to-end learning of geometry and context for deep stereo regression. In *Proc. of International Conference on Computer Vision (ICCV)*, pages 66–75, 2017.
- [21] Jernej Kos, Ian Fischer, and Dawn Song. Adversarial examples for generative models. In *2018 IEEE Security and Privacy Workshops, SP Workshops 2018, San Francisco, CA, USA, May 24, 2018*, pages 36–42, 2018.
- [22] Alexey Kurakin, Ian J. Goodfellow, and Samy Bengio. Adversarial examples in the physical world. In *ICLR (Workshop)*. OpenReview.net, 2017.
- [23] Yanpei Liu, Xinyun Chen, Chang Liu, and Dawn Song. Delving into transferable adversarial examples and black-box attacks. In *5th International Conference on Learning Representations, ICLR 2017, Toulon, France, April 24-26, 2017, Conference Track Proceedings*, 2017.
- [24] Aleksander Madry, Aleksandar Makelov, Ludwig Schmidt, Dimitris Tsipras, and Adrian Vladu. Towards deep learning models resistant to adversarial attacks. In *6th International Conference on Learning Representations, ICLR 2018, Vancouver, BC, Canada, April 30 - May 3, 2018, Conference Track Proceedings*, 2018.
- [25] Moritz Menze and Andreas Geiger. Object scene flow for autonomous vehicles. In *Proc. of IEEE Conference on Computer Vision and Pattern Recognition (CVPR)*, 2015.
- [26] Alejandro Newell, Kaiyu Yang, and Jia Deng. Stacked hour-glass networks for human pose estimation. In *Proc. of European Conference on Computer Vision (ECCV)*, pages 483–499. Springer, 2016.
- [27] N.Mayer, E.Ilg, P.Häusser, P.Fischer, D.Cremers, A.Dosovitskiy, and T.Brox. A large dataset to train convolutional networks for disparity, optical flow, and scene flow estimation. In *Proc. of IEEE Conference on Computer Vision and Pattern Recognition (CVPR)*, 2016. arXiv:1512.02134.
- [28] Nicolas Papernot, Patrick D. McDaniel, Ian J. Goodfellow, Somesh Jha, Z. Berkay Celik, and Ananthram Swami. Practical black-box attacks against machine learning. In *Proceedings of the 2017 ACM on Asia Conference on Computer and Communications Security, AsiaCCS 2017, Abu Dhabi, United Arab Emirates, April 2-6, 2017*, pages 506–519, 2017.
- [29] Nicolas Papernot, Patrick D. McDaniel, Xi Wu, Somesh Jha, and Ananthram Swami. Distillation as a defense to adversarial perturbations against deep neural networks. In *IEEE Symposium on Security and Privacy*, pages 582–597. IEEE Computer Society, 2016.
- [30] Anurag Ranjan, Joel Janai, Andreas Geiger, and Michael J. Black. Attacking optical flow. In *International Conference on Computer Vision (ICCV)*, 2019.
- [31] Jérôme Rony, Luiz G. Hafemann, Luiz S. Oliveira, Ismail Ben Ayed, Robert Sabourin, and Eric Granger. Decoupling direction and norm for efficient gradient-based L2 adversarial attacks and defenses. In *IEEE Conference on Computer Vision and Pattern Recognition, CVPR 2019, Long Beach, CA, USA, June 16-20, 2019*, pages 4322–4330, 2019.
- [32] Daniel Scharstein, Heiko Hirschmüller, York Kitajima, Greg Krathwohl, Nera Nešić, Xi Wang, and Porter Westling. High-resolution stereo datasets with subpixel-accurate ground truth. In *German conference on pattern recognition*, pages 31–42. Springer, 2014.
- [33] Daniel Scharstein and Richard Szeliski. A taxonomy and evaluation of dense two-frame stereo correspondence algorithms. *International Journal of Computer Vision*, 2002.
- [34] Ludwig Schmidt, Shibani Santurkar, Dimitris Tsipras, Kunal Talwar, and Aleksander Madry. Adversarially robust generalization requires more data. In *Proceedings of the 32nd International Conference on Neural Information Processing Systems*, pages 5019–5031, 2018.
- [35] Mahmood Sharif, Sruti Bhagavatula, Lujo Bauer, and Michael K. Reiter. Accessorize to a crime: Real and stealthy attacks on state-of-the-art face recognition. In *Proceedings of the 2016 ACM SIGSAC Conference on Computer and Communications Security, Vienna, Austria, October 24-28, 2016*, pages 1528–1540, 2016.
- [36] Christian Szegedy, Wojciech Zaremba, Ilya Sutskever, Joan Bruna, Dumitru Erhan, Ian J. Goodfellow, and Rob Fergus. Intriguing properties of neural networks. In *ICLR*, 2014.
- [37] Richard Szeliski. *Computer vision: algorithms and applications*. Springer Science & Business Media, 2010.
- [38] Alex Wong, Mukund Mundhra, and Stefano Soatto. Stereopagnosia: Fooling stereo networks with adversarial pertur-

- bations. In *Proceedings of the AAAI Conference on Artificial Intelligence*, volume 35, 2021.
- [39] Cihang Xie, Jianyu Wang, Zhishuai Zhang, Yuyin Zhou, Lingxi Xie, and Alan L. Yuille. Adversarial examples for semantic segmentation and object detection. In *IEEE International Conference on Computer Vision, ICCV 2017, Venice, Italy, October 22-29, 2017*, pages 1378–1387, 2017.
- [40] Cihang Xie, Yuxin Wu, Laurens van der Maaten, Alan L. Yuille, and Kaiming He. Feature denoising for improving adversarial robustness. In *IEEE Conference on Computer Vision and Pattern Recognition, CVPR 2019, Long Beach, CA, USA, June 16-20, 2019*, pages 501–509, 2019.
- [41] Cihang Xie, Zhishuai Zhang, Yuyin Zhou, Song Bai, Jianyu Wang, Zhou Ren, and Alan L. Yuille. Improving transferability of adversarial examples with input diversity. In *IEEE Conference on Computer Vision and Pattern Recognition, CVPR 2019, Long Beach, CA, USA, June 16-20, 2019*, pages 2730–2739, 2019.
- [42] Kyle Yee and Ayan Chakrabarti. Fast deep stereo with 2d convolutional processing of cost signatures. In *Proceedings of the IEEE/CVF Winter Conference on Applications of Computer Vision (WACV)*, March 2020.
- [43] Jure Zbontar and Yann LeCun. Stereo matching by training a convolutional neural network to compare image patches. *Journal of Machine Learning Research*, 2016.
- [44] Feihu Zhang, Victor Prisacariu, Ruigang Yang, and Philip HS Torr. Ga-net: Guided aggregation net for end-to-end stereo matching. In *Proc. of IEEE Conference on Computer Vision and Pattern Recognition (CVPR)*, 2019.
- [45] Zekun Zhang and Tianfu Wu. Learning ordered top-k adversarial attacks via adversarial distillation. In *Proceedings of CVPR 2020 Workshop on Adversarial Machine Learning in Computer Vision*, 2020.